Pergamon

Acta Materialia 50 (2002) 1507–1522

Acta MATERIALIA

www.actamat-journals.com

Numerical simulations of hydrogen–dislocation interactions in *fcc* stainless steels. Part I: hydrogen–dislocation interactions in bulk crystals

J.P. Chateau [a], D. Delafosse [b,*], T. Magnin [b]

[a] *Present address: LPM, Ecole des Mines, Parc de Saurupt, 54042 Nancy cedex, France*

[b] *Centre Science des Matériaux et des Structures, CNRS PECM, Ecole Nationale Supérieure des Mines de Saint-Etienne, 158 Cours Fauriel, 42023 Saint-Etienne cedex 02, France*

Received 25 April 2001; received in revised form 6 December 2001; accepted 6 December 2001

Abstract

The basic equations for the coupling between stress and hydrogen diffusion are presented. A numerical simulation method is proposed. It is based on the diffusion equation including a hydrostatic stress gradient term, and on a discretisation of the hydrogen concentration field. The simulation scheme is applied to elementary dislocation configurations in order to compute the influence of solute hydrogen on dislocation interactions. A simple general expression is derived for the hydrogen screening effect on the pair interactions between co-planar dislocations. This expression is used to investigate the influence of diffusing hydrogen on the cross-slip probability of screw dislocations. First numerical results are presented. They are discussed in relation with the modelling of transgranular stress corrosion crack propagation.

Résumé

Les équations régissant le couplage entre la contrainte et la diffusion de l'hydrogène sont presentées. Nous proposons une méthode de simulation numérique qui repose sur l'équation de la diffusion incluant un terme de gradient de contrainte hydrostatique et sur une discrétisation du champ de concentration en hydrogène. La méthode de simulation est appliquée à des configurations de dislocations élémentaires pour lesquelles nous calculons l'effet de l'hydrogène en solution sur les interactions entre dislocations. Nous dérivons une expression générale simple qui exprime l'effet de l'hydrogène sur l'écrantage des interactions de paires entre dislocations coplanaires. Cette expression est utilisée pour étudier l'influence de la diffusion de l'hydrogène sur la probabilité de glissement dévié des dislocations vis. Ces premiers résultats sont discutés dans la perspective de leur application à l'étude par simulation numérique de la propagation transgranulaire de fissures de Corrosion Sous Contrainte.

Keywords: Hydrogen embrittlement; Austenitic steels; Dislocation; Stress corrosion

1359-6454/02/$22.00
PII: S1359-6454(02)00008-3

1. Introduction

Although the phenomenon of Stress Corrosion Cracking (SCC) has been well documented for over a century in many engineering material/solution systems, successful predictive approaches of this type of damage are still scarce. In order to address such an important issue, the physical modelling of SCC phenomena has received much attention during the past decade. During this decade, a consensus was reached about the essential role played by corrosion–deformation interaction effects (see [1] for a review and [2] for recent contributions). Among the various proposed mechanisms, hydrogen induced plasticity and damage is increasingly invoked in many material/solution systems susceptible to SCC [3–6]. However, a significant gap remains between phenomenological models lying at the scale of the elementary crystallographic fracture facet (typically 1 μm), and macroscopic SCC experiments. Numerical simulations aimed at quantifying the elementary processes invoked in different models are a promising way of achieving such a scale change by connecting local quantities to measurable macroscopic parameters.

Numerous recent experimental results highlight hydrogen effects on plasticity that are in agreement with the Hydrogen Enhanced Localised Plasticity (HELP) model for hydrogen-assisted fracture [7–9]. More recently, the Corrosion Enhanced Plasticity Model (CEPM) was proposed to account more specifically for SCC fracture mechanisms in *fcc* alloys [10]. Both models invoke a localised 'hydrogen softening' effect, originating in the screening of hydrostatic stress centres by solute hydrogen. Sofronis and Birnbaum have provided a detailed finite element analysis of such effects, based on the coupled elasticity–diffusion equations [11,12].

In this paper, we propose an alternative numerical approach to this problem, which is aimed at the introduction of solute hydrogen effects in discrete dislocation dynamics simulations, especially for crack-tip plasticity problems. We first recall the basic equations for the coupled elasticity–diffusion problem and describe the proposed numerical method for computing hydrogen effects. Section 3 is dedicated to the testing of the method on elementary dislocation configurations. First simulation results are discussed in Section 4, in conjunction with the complex issue of the 'softening' versus 'hardening' of crystals by solute hydrogen. Conclusions are drawn concerning the application of the simulation scheme to crack tip plasticity problems, which is the subject of the second part of this paper.

* Corresponding author. Tel./fax: +33-4-7742-0298.
E-mail address: delafosse@emse.fr (D. Delafosse).

2. First order coupling between elasticity and hydrogen diffusion

Sofronis and Birnbaum [11,12] have given a thorough treatment of the coupled elasticity–diffusion problem for hydrogen in solid solution, in conjunction with the HELP (Hydrogen Enhanced Localised Plasticity) model for hydrogen-assisted cracking. Our approach is identical in terms of the basic equations for the coupling between elasticity and diffusion, but the numerical method and the discretisation scheme are different from their finite-element analysis. This method is designed to fit in a general simulation framework, based on the elastic theory of discrete dislocations. In this section, we recall the basic equations of hydrogen coupled diffusion–elasticity, and we present a numerical method based on a discretisation of the hydrogen distribution for computing the hydrogen–dislocation interaction forces.

2.1. Stress assisted diffusion of hydrogen

Solid solution hydrogen diffuses in the host metal in interstitial sites (octahedral sites in austenitic steel at room temperature). Its small size allows for a higher solubility and a greater mobility than other elements. However, hydrogen atoms are larger than the interstitial sites: $r_H = 0.53$ Å, to be compared with $r_i = 0.19$ Å for octahedral sites in austenitic steel. This induces a distortion of the host lattice. The resulting stress and displacement fields interact with other defects. This is expressed

by hydrogen's partial molar volume, i.e. the unconstrained volume dilatation of the metal containing one mole of hydrogen. A typical value is $V* = 2\ cm^3/mol$ for *fcc* materials [13]. An isochore introduction of hydrogen into a lattice creates a hydrostatic compression stress. Thereby, the mean hydrostatic stress affects the hydrogen solubility in the host metal, and hydrostatic stress gradients affect hydrogen diffusion.

The chemical potential of hydrogen is the energy required to move a hydrogen atom from infinity into the lattice. Let σ be the total stress tensor, $\mathbf{H}$ the expansion tensor of a hydrogen atom, C_0 the volume concentration (mol/m^3) in the initial reference state, and C the concentration in the current state. The primary cause for the elastic interaction between hydrogen and hydrostatic stress fields is a first-order dilatational interaction, which alters the chemical potential per hydrogen atom [12]:

$$\mu = \mu_0 + kT \ln\left(\frac{C}{C_0}\right) - H_{ij}\sigma_{ij} \tag{1}$$

where μ_0 is the chemical potential at initial concentration equal to C_0, k is Boltzmann's constant and T the temperature. The total chemical potential is lowered by the elastic energy resulting from the interaction between the strain induced by hydrogen and the stress field in the material. The strain due to a local hydrogen concentration C is given by:

$$\varepsilon_{ij}^{H} = \mathbf{H}_{ij}(C - C_0)N_{\mathrm{av}} \tag{2}$$

where $\mathbf{H}$ is the expansion strain tensor of one hydrogen atom and N_{av} is the Avogadro number. When a concentration C of hydrogen is introduced, the unconstrained dilatation volume is:

$$\mathrm{e}^{H} = (C - C_0)V^* \tag{3}$$

It induces hydrostatic strains, and the corresponding strain tensor is:

$$\varepsilon_{ij}^{H} = \frac{1}{3}(C - C_0)V^*\delta_{ij} \tag{4}$$

where δ is the Kronecker delta. By injecting Eqs. (2) and (4) into Eq. (1), the chemical potential becomes:

$$\mu = \mu_0 + kT \ln\left(\frac{C}{C_0}\right) - \frac{V^*}{N_{\mathrm{av}}}\frac{\sigma_{kk}}{3} \tag{5}$$

The local flux (in $mol\ m^{-2}\ s^{-1}$) is given by:

$$\mathbf{J} = -\frac{DC}{kT}\nabla\mu \tag{6}$$

where D is the diffusion coefficient of hydrogen at temperature T. Combining Eqs. (5) and (6), one obtains a modified expression of the first Fick's law containing a 'source' term proportional to the trace of the stress tensor (hydrostatic stress):

$$\mathbf{J} = -D\cdot\nabla C + \frac{DV^*}{RT}\cdot C\cdot\nabla\frac{\sigma_{kk}}{3} \tag{7}$$

R is the perfect gas constant. By differentiation, the second Fick's law comes:

$$\frac{\partial C}{\partial t} = D\cdot\nabla^2 C - \frac{DV^*}{RT}\left[C\cdot\nabla^2\frac{\sigma_{kk}}{3} + \nabla C\cdot\nabla\frac{\sigma_{kk}}{3}\right] \tag{8}$$

Relation (5) indicates that the energy necessary to introduce a hydrogen atom in the lattice is increased by the previous presence of hydrogen and decreased by hydrostatic dilatation stress. In other words, the interaction between hydrogen-induced strains and a hydrostatic stress σ amounts to a binding energy $W_{\mathrm{int}} = -\sigma V^*$ per hydrogen mole. Eqs. (6)–(8) are used to compute the diffusion of hydrogen within the stress field induced by other defects. They are identical to those used by Van Leeuwen to study hydrogen diffusion at a loaded crack tip [14]. The local flux depends on the concentration and hydrostatic stress gradients. Hydrogen diffuses towards zones in tension and relaxes the hydrostatic stress, as shown in the following.

2.2. Hydrostatic stress relaxation

The local hydrostatic stress $\sigma_{kk}/3$ in Eq. (6) is the sum of the stresses due to all dilatation sources in the material, including hydrogen. Considering an infinite matrix containing an initially uniform hydrogen concentration C_0, a local change $(C - C_0)$ of concentration induces hydrostatic stresses. We determine this stress by using Eshelby's results for an inclusion [15]. Cutting a volume element Ω out of the matrix with uniform concentration C_0 and increasing its hydrogen content up to C results in an unconstrained dilatation strain ε^H given by

Eq. (4). Then, inserting Ω back into the initial cavity requires the application of a compatibility strain $\varepsilon^{\text{elast}}$ to compensate for the unconstrained dilatation. The total strain inside Ω becomes:

$$\varepsilon^{\Omega} = \varepsilon^{\text{elast}} + \varepsilon^{H} \tag{9}$$

$\varepsilon^{\text{elast}}$ is the elastic strain imposed by the matrix, such that ε^{Ω} fulfils the compatibility equation at the element/matrix interface. Eshelby's results give the expression for the total strain, deduced from the unconstrained strain due to hydrogen:

$$\varepsilon^{\Omega} = S{:}\varepsilon^{H} \tag{10}$$

where S is Eshelby's tensor. For a purely dilatational strain, Eq. (10) reduces to:

$$\varepsilon_{11}^{\Omega} = \varepsilon_{22}^{\Omega} = \varepsilon_{33}^{\Omega} = \frac{1+\nu}{3(1-\nu)}\varepsilon_{11}^{H} \tag{11}$$

Eq. (11) and Hooke's law give the expression of the stress due to the elastic strain:

$$\sigma_{11}^{H} = -\frac{E}{1-2\nu}\left[\frac{1+\nu}{3(1-\nu)}-1\right]\varepsilon_{11}^{H} = \sigma_{22}^{H} = \sigma_{33}^{H} \tag{12}$$

Hence, the induced stress inside Ω is hydrostatic, and Eqs. (4) and (12) give:

$$\frac{\sigma_{kk}^{H}}{3} = -\frac{2EV^{*}}{9(1-\nu)}(C-C_0) \tag{13}$$

which is the expression for the local hydrostatic stress due to a local concentration C varying from C_0. In an infinite matrix, the hydrostatic stress induced outside Ω is zero. Thus, the stress due to hydrogen only depends on the local concentration. The total hydrostatic stress appearing in the diffusion law (Eq. (7)) is the sum of the dislocations' contribution (Eq. (A9)Eq. (B5)) and of the stress due to hydrogen (Eq. (13)). Straight perfect screw dislocations do not induce any hydrostatic stress. Hydrogen only interacts to first order with dislocations having a non-zero edge component.

2.3. Second order interactions

In addition to this first order elastic interaction, a second-order term stems from a change in the elastic moduli caused by the presence of hydrogen inside a volume element v. If C'_{ijkl} and C_{ijkl} are the elastic constants, respectively with and without hydrogen, the second order interaction energy is [16]:

$$W'_{\text{int}} = \frac{1}{2}(C'_{ijkl}-C_{ijkl})\varepsilon'_{ij}\varepsilon_{kl}v \tag{14}$$

where ε'_{ij} are the elastic strains inside v after the solute atoms were introduced while the external stress was held constant and ε_{kl} are the strains caused by the external stress in the absence of solute atoms. Even a small alteration of the elastic constants can be expected to have important consequences near stress singularities such as dislocations. However, as it scales like $1/r^2$, compared to the $1/r$ dependence for the first order interaction, it only has a significant effect on the concentration profile near the dislocation core [11]. Hydrogen is expected to interact with straight screw segments via this second order term and In situ environmental TEM measurements of dislocation velocities show that solute hydrogen affects the mobility of dislocations regardless of their character [8].

This non-linear second level of coupling is neglected in our approach and only the first order 'volumetric' effects are considered because in the present SCC model, the crack–dislocation configuration considered is two-dimensional, with a straight crack shielded by an array of parallel edge dislocations (cf. part II). In such a configuration, the effect of hydrogen on parallel edge dislocations mainly derives from the first order interactions. Sofronis and Birnbaum [12] show that the second level of coupling accounts for 10% of the interaction force between hydrogen and edge dislocations, which gives a net effect of about 2–4% of the total force on a dislocation for high hydrogen concentrations (see Section 3.2).

In the next section, we detail the discretisation method used for computing in two dimensions the first order interaction between hydrogen and edge dislocations.

2.4. Computation of the first order interactions

In order to study the elastic interactions between hydrogen and edge dislocations, one has to evaluate both the diffusion of hydrogen in the stress field

of the dislocations and the resulting forces exerted by hydrogen on the dislocations. To compute hydrogen diffusion in two dimensions, we mesh the complex plane around the dislocations with a square grid having a few nanometre cell-size. Two different methods may be used:

1. Transient diffusion: introducing an elementary time increment, we solve the diffusive initial value problem for local hydrogen fluxes given by Eqs. (7) and (13). At each time step the variation of hydrogen concentration in each box[1] is computed and the stress relaxation due to hydrogen segregation is updated. This method is used with moving dislocations or when a fixed hydrogen flux is imposed as a boundary condition, modelling for instance a cathodic hydrogen discharge at a stress corrosion crack tip. An example of such a simulation is presented in part II.
2. Steady state distribution: in the elementary cases presented in this paper, we study the stationary hydrogen distribution around fixed dislocations within an initially uniform concentration field. When the diffusion time tends to infinity, the distribution of hydrogen around the dislocations tends to a steady state, defined by $\mathbf{J} = 0$. The spatial integration of Eq. (7) between infinity and the current position then gives the expression of the local concentration:

$$C = C_0 \exp\left\{\frac{V^*}{RT}\left[\frac{(1+\nu)}{3}(\sigma_{11}+\sigma_{22}) - \frac{2EV^*}{9(1-\nu)}(C-C_0)\right]\right\}. \quad (17)$$

The solution C of this equation is computed numerically at each grid node by a Newton-type of iteration. This yields the Cottrell expression [17] for the segregation of solute atoms around dislocations:

$$\frac{c}{1-c} = \frac{c_0}{1-c_0}\exp\left(-\frac{W_{\text{int}}}{kT}\right) \quad (18)$$

where c is the atomic concentration n_H/n_M. The resulting hydrogen profile is either called in the following the distribution 'in equilibrium with the local stress', or the 'stationary' or 'steady state' distribution.

The hydrogen–dislocations interaction force results from the lattice distortion at the atomic scale. Each hydrogen solute atom acts as a point source of expansion whose displacement field in three dimensions is radial. To compute the stress induced by hydrogen solute atoms at the scale of dislocations, we use the same space discretisation as for the diffusion problem. We thus evaluate the stress due to all hydrogen atoms present in one diffusion box by assuming that these atoms are concentrated along a line at the centre of the box (Fig. 1). In this respect, each box has an equivalent line defect: a dilatation line perpendicular to the simulation plane. The strength of such a defect depends on the distance between the solute atoms along the line and is proportional to the local concentration in the box. This allows for the handling of the hydrogen distribution as a collection of discrete line defects, just like dislocations. From St Venant's and the principle of superposition in linear elasticity, we evaluate the total stress due to a dispersal of hydrogen by summing over the equivalent discrete distribution of dilatation lines.

The stress field of an individual dilatation line has a cylindrical symmetry, in agreement with the plane strain assumption made for dislocations. Its determination is detailed in Appendix A. The expressions are obtained in the complex plane, to allow for the same use as for dislocations in the vicinity of a crack (complex potentials, interaction forces, and boundary conditions) [18]. At a position z in the complex plane, the stress field of the dilatation line associated with box j is given by:

$$\begin{cases} \sigma_{11} + \sigma_{22} = 0 \\ \sigma_{22} + i\cdot\sigma_{12} = \dfrac{B_j}{s(z-\xi_j)^2} \text{ where } B_j = \dfrac{\mu V^* C_j h^2}{2\pi(1-\nu)} \end{cases} \quad (19)$$

ξ_j is the complex position of the line, C_j is the local

[1] In the following, the term 'box' or 'cell' denote the square area of width h surrounding each grid node.

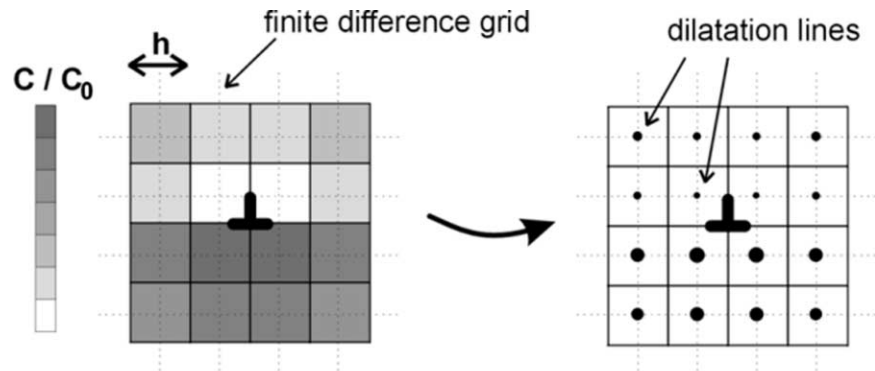

Fig. 1. Schematic representation of the discretisation scheme for the hydrogen concentration field. (left): The diffusion equation is solved numerically using a finite difference method on a uniform grid with square cells of width h. (right): The resulting hydrogen distribution is transformed into a discrete distribution of line sources of expansion ('dilatation lines') located at the centre of each grid cell. Their magnitude is proportional to the hydrogen concentration in the cell.

concentration in the box, h is the box width, and $i^2 = -1$. The stress field of a dilatation line scales with $1/r^2$ and decreases rapidly. One may notice that in Eq. (19), the hydrostatic stress is zero. This shows that there is no elastic interaction between the dilatation lines, validating the assumption made in Eq. (13) that the hydrostatic stress relaxation in a box only depends on the local hydrogen concentration.

The force exerted by a dilatation line on a dislocation is detailed in Appendix B, and the total force due to the distribution of hydrogen is computed as the sum over all the dilatation lines. The total force exerted by n dilatation lines at positions ξ_j with local concentration C_j, on a dislocation at position ζ, is given by:

$$\bar{f}_{H/d} = \frac{\mu V^* h^2 b_e}{2\pi i(1-\nu)} \sum_{j=1}^{n} \frac{C_j}{(\zeta-\xi_j)^2} \tag{20}$$

where b_e is the complex edge component of the Burgers' vector of the dislocation. $\bar{f}_{H/d}$ is the conjugate of the force. This force also scales as $1/r^2$ and decreases rapidly. Nevertheless, since the total force on a dislocation is the sum over all the dilatation lines in the simulation area, hydrogen effects do not vanish at long distances, as shown in the following.

3. Hydrogen effects on elementary dislocation configurations

In this section, we apply the numerical method described above for computing the distribution in equilibrium with the local stress ('stationary distribution') to elementary dislocation configurations. The first order interactions are evaluated successively for one isolated, and for two co-planar edge dislocations. A general simple expression is then derived for the asymptotic value of the hydrogen effect on co-planar dislocations, and the particular case of a dissociated screw dislocation is investigated and discussed in conjunction with the influence of hydrogen on the cross-slip process.

3.1. One isolated edge dislocation: screening of the resolved shear stress

First, we study the hydrogen distribution and the associated stress field around a single edge dislocation. The dislocation is placed in an initially uniform concentration C_0. Fig. 2 shows the steady state distribution of hydrogen around the dislocation for an initial concentration equal to 0.01. The box size h is taken equal to $10b$ (b: Burgers' vector of the dislocation). The simulation area is a square of 20×20 boxes, centred at the dislocation

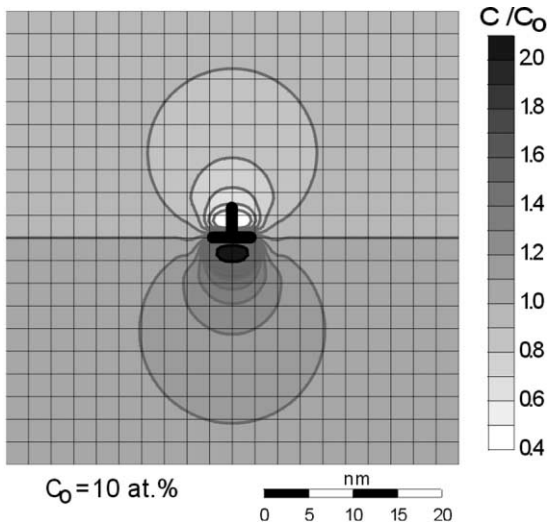

Fig. 2. (a) Equilibrium hydrogen distribution around a single edge dislocation at $T = 390$ K in a 316L austenitic stainless steel in a uniform remote concentration. The hydrogen distribution maps the contours of the hydrostatic stress with a depletion on the 'upper' side of the dislocation (compression) and a segregation on the 'lower' side of the glide plane (tensile zone).

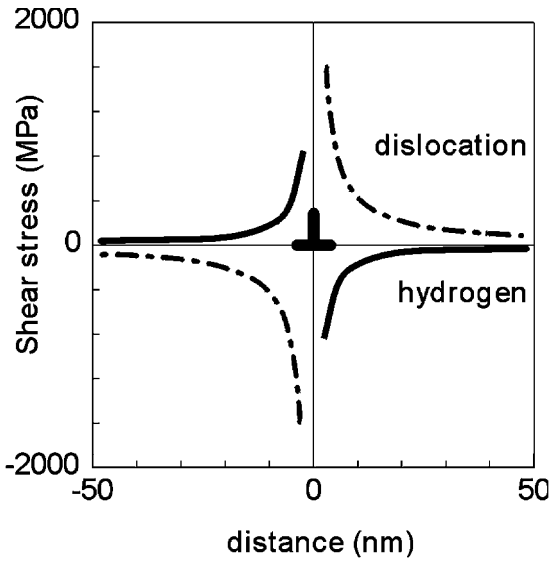

Fig. 3. Shear stress profile along the glide plane of an isolated edge dislocation. The sum of the dilatation strains due to the non-symmetric distribution of hydrogen (Fig. 2) yields a shear stress profile opposed to that of the dislocation. The net effect is a relaxation of the resolved shear stress of the dislocation.

position. Numerical data used are: $\mu = 75$ GPa, $\nu = 0.275$, $b = 2.55$ Å, $V* = 2\text{cm}^3\ \text{mol}^{-1}$ and $D = 5.3 \times 10^{-10}\text{cm}^2\ \text{s}^{-1}$ at $T = 390$ K, which correspond to the experimental conditions for the SCC of 316L single crystals in a boiling $MgCl_2$ solution [10]. Predictably, the contours of the hydrogen distribution in equilibrium with the local stress precisely map those of the hydrostatic stress field associated with an edge dislocation. Transient diffusion computations at 390 K showed that the steady state distribution was approached for a physical time of 10^{-3} s. The asymmetrical distribution of hydrogen with respect to the slip plane induces a negative shear stress component in the slip plane. It is computed using the dilatation line method. Fig. 3 displays the shear component induced in the slip plane as a function of the distance to the dislocation core. It exhibits the same singularity as that of the mere dislocation, but with opposite sign and a weaker amplitude. Segregating hydrogen induces a resolved shear stress opposed to that of the dislocation. The net effect is a decrease of the resolved shear stress of the edge dislocation.

3.2. Two co-planar edge dislocations: screening of the interaction force

If we place a second edge dislocation in the slip plane of the first dislocation, after Peach and Köhler's relation, one can expect a decrease of the interaction force between the two dislocations. Two edge dislocations with the same Burgers' vector and slip plane are inserted in an initially uniform distribution of hydrogen. At steady state, the segregation ratio of hydrogen is higher than in the case of a single dislocation. The hydrostatic stress fields of both dislocations superimpose and the maximum concentration near a dislocation increases as the distance between the dislocations decreases.

The total glide force on one of them is plotted against the distance (Fig. 4), for the same data as in Section 3.1. When the dislocations are separated by more than four boxes (10 nm), the relative decrease in the interaction force is shown to remain constant with the distance. For initial proportions of hydrogen rising from 0.01 to 0.1, 7 to 38% of the interaction force is shielded in austenitic stain-

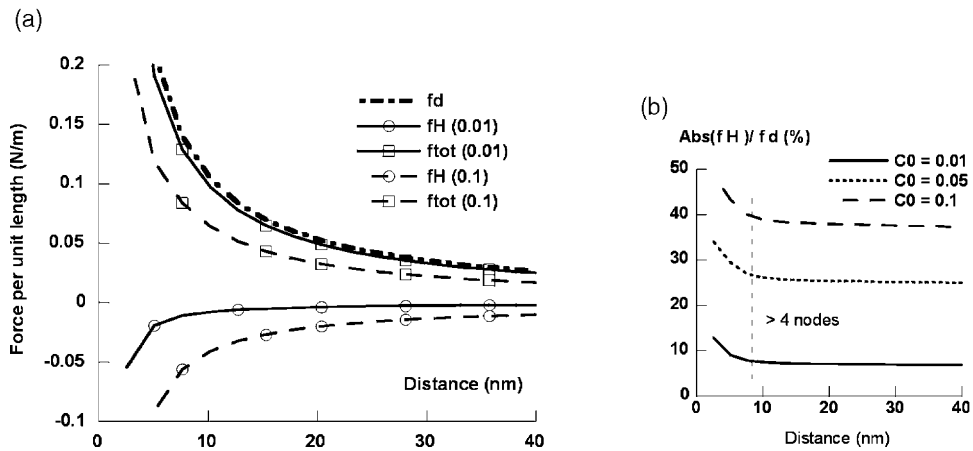

Fig. 4. Interaction forces between two coplanar dislocations, as a function of the separation distance and remote hydrogen concentration. (a): Peach & Köhler's force (f_d), hydrogen component (f_H), and total force ($f_{tot} = f_d + f_H$) in the presence of hydrogen in mean concentration 0.01 and 0.1. (b): The *relative* screening of the pair interactions $|f_H/f_d|$ increases with the mean concentration and is nearly constant with the separation distance, provided four grid nodes at least separate the two dislocations (10 nm. in this example).

less steel at 390 K. This reduction of the pair interactions is at the root of the so-called 'softening' phenomenon in hydrogen-containing alloys. From a macroscopic point of view, the 'softening' versus 'hardening' of alloys by solid solution hydrogen is a complex—sometimes controversial—issue, which was extensively discussed elsewhere [6,8]. The term 'screening' might be more relevant to denote this effect at the dislocation level and will be used in the remainder of this paper.

3.3. Effect of temperature and concentration: general expression for the screening effect

Temperature influences the transient diffusion of hydrogen. It increases its kinetics, via the increase of the diffusion coefficient. Eq. (17) shows that it also has a strong influence on the stationary hydrogen distribution. Solving this equation numerically, we can see that the effect of temperature depends on the initial concentration. Table 1 shows the dependence of the segregation ratio C/C_0 at $2b$ under the dislocation, for two initial concentrations and various temperatures. The distance $2b$ corresponds to a core cut-off for hydrogen–dislocation interactions: at that distance in a 316L steel, the hydrostatic stress is equal to 7000 MPa, which corresponds to a binding energy $W_{int} = -\sigma V^*$ equal to -14 kJ mol^{-1}, a value experimentally measured in austenitic stainless steels [19]. For small initial amounts of hydrogen, dislocations tend to be saturated at low temperature, while for a high initial amount, the segregation ratio is lower. High temperatures tend to smooth the hydrogen distribution.

The net effect of the initial concentration and temperature on the hydrogen screening effect is investigated numerically. The situation of two fixed dislocations separated by $100b$ is studied for a concentration $c = n_H/n_M$ and a temperature T varying within the ranges $2\cdot10^{-3}$–0.1 and 20–600 K. Fig. 5 shows the relative decrease of the pair interaction S(%) (called the 'screening index' in the following) at steady state. The screening effect increases with increasing initial concentration and decreasing temperature, these two parameters playing an inverse role. A numerical best fit procedure leads to an expression of $S = f(c,T)$ with the following simple form:

$$S = \frac{S_0}{1 + \beta\frac{T}{c}} \tag{21}$$

S_0 is found to amount to 75% and β to 2.5 10^{-4} K^{-1}. S_0 is the asymptotic value of the screening index at 0 K (if hydrogen was allowed to diffuse at this temperature). We conducted the same pro-

Table 1
Hydrogen segregation ratio c/c_0 at a distance $2b$ from the dislocation core, as a function of the remote hydrogen concentration c_0 and temperature

		Temperature (K)					
		100	200	300	390	500	600
c_0	0.002	149	97	58	36	22	13
	0.1	4.83	4.48	4.15	3.90	3.61	3.38

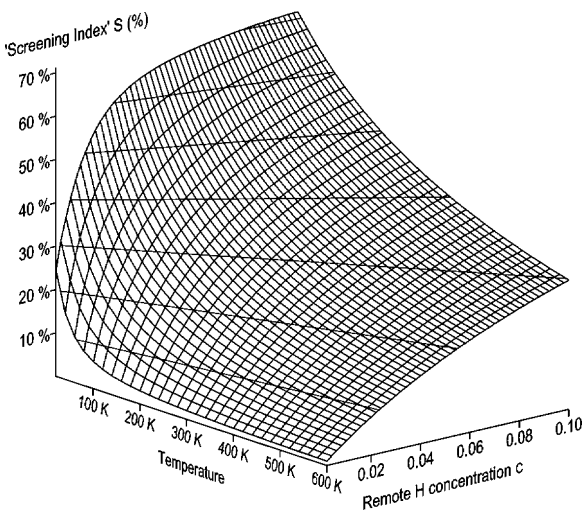

Fig. 5. Screening index S(%) as a function of temperature T and mean hydrogen concentration c. Interactions between two coplanar edge dislocations in a 316L austenitic stainless steel (simulation results). The two parameters are seen to play a reciprocal role, and the largest decrease of the pair interactions (75%) is obtained asymptotically at 0 K.

cedure with materials parameters corresponding to nickel and aluminium. It showed that S_0 does not depend on the material constants and is always equal to 75%. At 0 K, the solution of Eq. (17) tends toward:

$$C-C_0 = \frac{9(1-\nu)}{2EV^*}\sigma^d \text{ where } \sigma^d = \frac{(1+\nu)}{3}(\sigma_{11}+\sigma_{22}) \tag{22}$$

This means that for a sufficient initial amount of hydrogen, the steady state would be reached when the relaxation of the hydrostatic stress is complete. A dimensional analysis shows that indeed, S_0 does not depend on the material constants. At $T\neq 0$ K, the concentration profile is given by Eq. (17). At high temperature, the solution can be linearised $(1/T\rightarrow 0)$:

$$C\cong C_0\left(1+\frac{V^*\sigma^d}{RT}-\frac{2EV^{*2}}{9(1-\nu)RT}(C-C_0)\right) \tag{23}$$

This gives:

$$C-C_0\cong C_0\frac{\dfrac{V^*\sigma^d}{RT}}{1+\dfrac{2EV^{*2}}{9(1-\nu)RT}C_0} \tag{24}$$

The profile defined by Eq. (22) leads to a screening index S_0 at 0 K. Thus, by a rule of three, the profile given by Eq. (24) leads to a screening index:

$$S\cong\left(S_0\frac{1}{\dfrac{9(1-\nu)}{2EV^*}}\right)C_0\frac{\dfrac{V^*}{RT}}{1+\dfrac{2EV^{*2}}{9(1-\nu)RT}C_0} \tag{25}$$

This gives a general expression for screening index S with the same form as previously found by a numerical best fit (Eq. (21)):

$$S=\frac{75\%}{1+\beta\dfrac{T}{c}} \text{ with } \beta=\frac{9(1-\nu)RV_M}{2EV^{*2}} \tag{26}$$

with E the Young's modulus, ν the Poisson's ratio and V_M the molar volume of the host metal. The coefficient β contains all the material parameters that influence the hydrogen screening effect as a function of the remote hydrogen concentration and

temperature. Eq. (26) was obtained for large values of C_0 and T, but since it has the same form as the fitted function Eq. (21), it is applicable over the whole range of concentration and temperature simulated. A comparison between the simulation results and the general Eq. (26) in the case of 316L is given on Fig. 6. The agreement between the two surfaces $S = f(c,T)$ is seen to be better than 2% over most of the investigated range. The largest discrepancy (~5%) was found near 0 K, where such a calculation is not physically relevant. The same assessments for nickel and aluminium give comparable results. We also compared the values given by Eq. (26) with those obtained by Sofronis and Birnbaum [12] by a coupled finite element analysis in Niobium (μ = 30.8 GPa, ν = 0.415, b = 2.85 Å, $V*$ = 1.88 cm^3 mol^{-1}, V_M = 10.8 cm^3 mol^{-1}, T = 300 K). In this case, Eq. (26) gives β = 7.67 10^{-4} K^{-1} and a 0.32%, 3.1% and 22.7% screening index, respectively for c = 0.001, 0.01 and 0.1, in agreement with their results.

3.4. One dissociated screw dislocation: hydrogen effect on the cross slip probability

A peculiar situation of dislocation interactions is the dissociation of a screw dislocation, which governs the cross slip process. This parameter will be of prior importance when we consider the formation of dense pile-ups leading to micro-fracture at a stress corrosion crack tip. A perfect screw dislocation dissociates into two mixed partials, separated by a stacking fault ribbon. Only the perfect screw dislocation can cross slip. This mechanism is thermally activated and the cross slip probability depends on the work necessary for the recombination of the partials. Each partial is submitted to two forces: the repulsion due to the other partial ($\alpha 1/r$) and the attraction due to the stacking fault (constant and equal to Γ, the Stacking Fault Energy: SFE). In the absence of external stress, the partials are in equilibrium at a distance where the two forces balance each other. It is observed experimentally that hydrogen promotes planar glide. The reason generally invoked is a decrease of the SFE [16,20], which induces an increase of the equilibrium distance and of the recombination work. Hirth and Lothe also suggest that it can interact elastically with the edge component of partial dislocations [16].

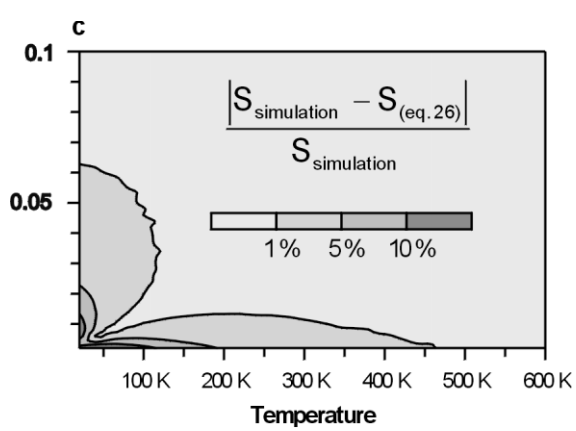

Fig. 6. Comparison between the 'screening index' $S = f(c,T)$ obtained by numerical simulation of the interactions at steady state (Fig. 5) and that given by the general expression (Eq. (26)). The largest discrepancy (>5%) is found near 0 K, where it is no longer physically relevant.

We studied this effect in nickel, which has an intermediate SFE value at room temperature (Γ = 100 mJ m^{-2}, $\Gamma/\mu b$ = 5.4 10^{-3}). Hydrogen only interacts with the edge component of the partials and decreases their interactions. Fig. 7 displays the equilibrium hydrogen distribution around two edge dislocations of opposite sign. Since the edge parts have opposite Burgers' vectors, they attract each other (the net repulsion is due to the leading repulsive contribution from the screw parts). Thus, by screening the attractive contribution, hydrogen increases the equilibrium distance, as well as the recombination work. Fig. 8 shows the evolution of the equilibrium distance and recombination work with the initial hydrogen concentration, in nickel at 300 K. We assumed a constant value of the SFE, in order to point out the elastic effect. The equilibrium distance was calculated directly by introducing the decrease of the interaction between the edge components (Eq. (26)). The recombination work was integrated between the equilibrium distance and b, the Burgers' vector of the perfect dislocation. The elastic effect of hydrogen promotes planar glide in nickel: for n_H/n_M = 0.05, as the equilibrium distance is increased by 25%, the recombination work is increased by 60%. Finally, one has to bear in mind

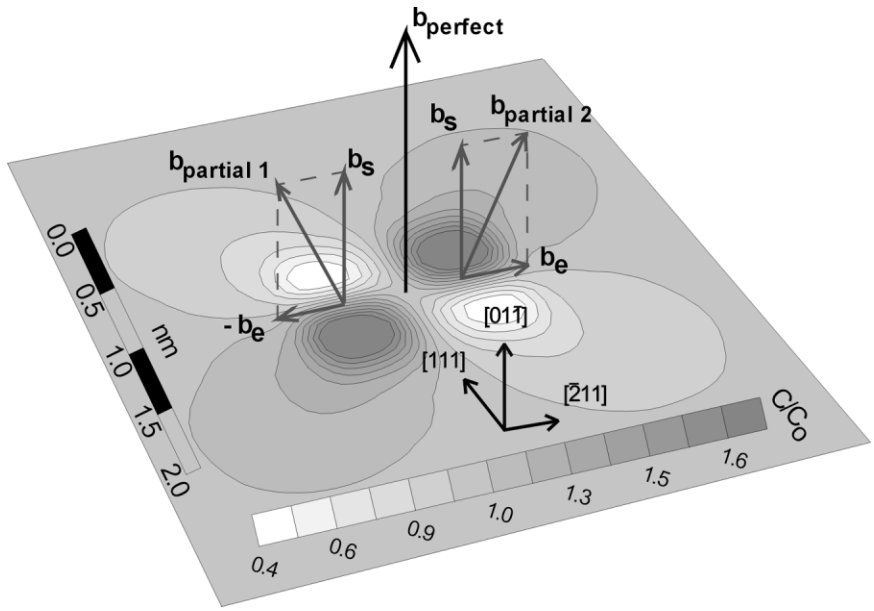

Fig. 7. Equilibrium hydrogen distribution around a dissociated screw dislocation in nickel ($c = 0.05$). Only the partial's edge component influences the hydrogen distribution to the first order. Hydrogen segregation results in a decrease of the attractive contribution to the interaction force (edge components of opposite sign), yielding a net repulsive effect on the partials.

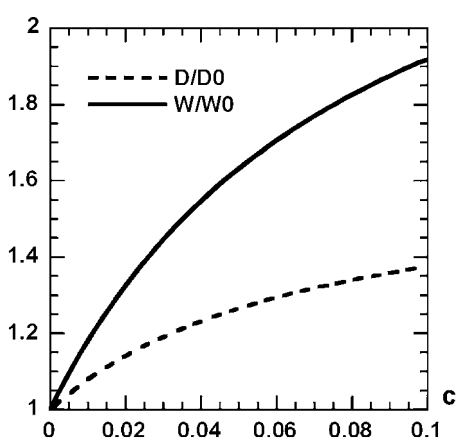

Fig. 8. Relative increase of the equilibrium dissociation distance (D/D_0) and constriction work (W/W_0) as a function of the hydrogen concentration (c) in nickel at 300 K, as predicted by Eq. (26).

that cross slip is a three dimensional process that operates via the constriction of the faulted ribbon [21]. Nevertheless, one can expect a relative effect of hydrogen on the appearance this constriction of the same order of magnitude as that obtained in 2D.

4. Discussion

The set of equations presented in Section 2 describes a 'classical' coupled problem of elasticity–diffusion. To handle this coupled problem along with discrete dislocations, our numerical method relies on the discretisation of the hydrogen distribution into a distribution of line defects superimposed to the diffusion grid. Meanwhile, dislocations remain discrete 2D objects in this approach. Their interactions can be treated analytically within the well-established framework of the elastic theory of discrete dislocations.

The independence of the results presented in Section 3 against the grid size was checked. It was found that the hydrogen effect on dislocation pair interactions was adequately described as soon as a minimum of four grid nodes separated the two dislocations. For closely spaced dislocations, this requirement may induce the evaluation of hydrogen concentration at a distance from the dislocation core where the relevance of linear elasticity can be questioned. As a matter of fact, the relevant scaling parameter for the influence of hydrogen on dislo-

cation interaction forces is the *magnitude of the 1/r singularity* of the hydrogen concentration profile, rather than the actual concentration level at a particular distance to the dislocation core. The correct numerical evaluation of the singularity amplitude requires a fine space discretisation between neighbouring dislocations.

The independence of the normalised hydrogen screening effect against the separation distance between dislocations enables one to express the hydrogen effect at saturation under the simple form given by Eq. (26). At a given temperature and remote hydrogen concentration, this expression gives an accurate estimate of the screening effect between parallel edge dislocations, provided the allowed diffusion time is sufficient to reach the steady state distribution. For *fcc* alloys at room temperature under monotonous straining, this condition is easily met at low and intermediate strain rates. In hydrogenated nickel for instance, the Portevin–Le Chatelier effect disappears around -30 °C [22–25], indicating that, at higher temperatures, the waiting time of mobile dislocations on forest obstacles is sufficient for dislocations to be nearly saturated by their hydrogen atmosphere during monotonic straining. However, this simple criterion is only valid in bulk crystals and the situation might be different at a SCC crack tip, where the boundary conditions for hydrogen diffusion are different.

The screening effect of solute hydrogen on dislocation interactions was clearly evidenced in various materials by means of environmental in situ Transmission Electron Microscopy (TEM) [26]. On the other hand, direct comparisons between the tensile curves of hydrogenated metals and their counterpart in hydrogen-free reference samples yields contradictory results that appear to be highly dependent on the nature of the host metal.

In *fcc* metals, dislocation pair interactions have an indirect contribution to the flow stress, via the multiplication/annihilation mechanisms and the evolution of the mobile and forest dislocation densities. In nickel, a macroscopic decrease of the flow stress was observed when the hydrogen screening of elastic interactions rather pertained to dislocation–solute interactions in Ni–C [27,28], or when a stable dislocation microstructure (Persistent Slip Bands) was previously build-up by cyclic plasticity in nickel single crystals [29]. In other alloys, such as austenitic stainless steels, a reduction of the strain hardening rate may be observed upon the introduction of solid solution hydrogen, but with a flow stress level consistently higher than that of hydrogen-free reference samples [30]. This indicates that other contributions to the flow stress are significantly affected by solute hydrogen. Generally, the extrapolation of two-dislocation mechanisms to the macroscopic tensile behaviour is not straightforward, particularly in *fcc* metals.

The evaluation of the first order hydrogen effect on the dissociation of a screw dislocation shows that it provides an efficient mechanism for impeding the cross-slip of screw dislocations. Recent experiments on nickel single crystals in low cycle fatigue show that solid solution hydrogen lowers the cross-slip probability [29]. This agrees qualitatively with early experiments by Windle and Smith on nickel single crystals in tension. They showed that τ_{III}—the resolved shear stress for the onset of stage III—was significantly increased by the presence of 400 ppm of hydrogen in solid solution [23]. The authors attributed this phenomenon to an estimated 35% decrease of the SFE due to hydrogen. However, the reference value they assumed in pure nickel (240 ergs cm^{-2} ($\equiv$mJ m^{-2})) was overestimated at least by a factor two. Nevertheless, these experiments pointed out a strong effect of a small amount of solid solution hydrogen on the cross slip probability.

Other available experimental results do not give a clear separation between these two possible categories of mechanisms (i.e. ‘elastic’ versus ‘core’ effects of hydrogen on dislocations). Ferreira et al. have estimated a 19% decrease of the SFE in a 310 austenitic stainless steel, by dislocation curvature measurements in an in situ environmental TEM [31]. However, their analysis neglected a possible alteration of the line tension in the presence of hydrogen. On the other hand, these authors interpreted the observed impeding effect of hydrogen on cross slip in aluminium as resulting from a decrease of the self-energy of edge segments [32]. Such an effect belongs to the ‘elastic’ category of candidate mechanisms, and should have direct consequences on the line tension of dislocations.

A critical review of the available results—possibly supplemented by quantitative experiments aimed at separating the various contributions—would be highly valuable and would give a more general insight to the competition between 'elastic' and 'core' effects of hydrogen on dislocation interaction mechanisms.

5. Summary and concluding remarks

Firstly, for 'volumetric' interactions between diffusing hydrogen and elementary dislocation configurations in two dimensions, the simulation method presented in this paper reproduces the results obtained by Sofronis and Birnbaum by finite element analysis:

- Hydrogen segregation in the hydrostatic stress field of edge dislocations and the resulting anti-symmetric stress relaxation with respect to the slip plane. This induces a decrease of the resolved shear stress associated with dislocations having a non-zero edge component.
- A decrease of the pair interactions between parallel edge dislocations. This decrease, like dislocation pair interactions, scales with the inverse of the separation distance. Consequently, when normalised by the dislocation pair interaction term, the 'screening' of the pair interactions was checked to be independent of the separation distance. This result was already pointed out by Sofronis for first order interactions (see Fig. 13 in [12]).

Secondly, this last result enables one to draw a simple, yet accurate to the first order, expression for the hydrogen screening effect on the interaction between co-planar dislocations (Eq. (26)). This expression can be useful for engineering purposes, giving the order of magnitude of the so-called 'hydrogen softening' effect that can be expected at a given temperature and mean hydrogen concentration.

However, as already emphasised, one must be very cautious invoking this 'softening' effect at a macroscopic scale.

Hydrogen effects on dislocations may also operate at the scale of local dislocation reaction mechanisms. An example is given by the study of the dissociated screw dislocation. It is shown how dislocation processes that involve elastic interactions between partial dislocations with an non-zero edge component of their Burger's vector can be altered by the presence of solute hydrogen. This 'elastic effect' has yet to be checked quantitatively against possible 'core effects' of hydrogen, such as a decrease of the SFE.

The numerical examples presented in this paper correspond to elementary configurations designed to assess the ability of the simulation method to handle discrete dislocation configurations. The results validate the relevance of our approach for two-dimensional configurations. Nevertheless, one should bear in mind that most dislocation reaction mechanisms are intrinsically 3D. In such situations, the type of two-dimensional approach presented here only gives a qualitative estimate of the hydrogen effects. On the other hand, a domain where the efficiency of using simplified 2D dislocation configurations was demonstrated is the physical modelling of crack–dislocation interactions for the study of the ductile to brittle transition. In the next part, we apply the present simulation scheme to this type of approach, in order to investigate the role of hydrogen on the Stress Corrosion Cracking mechanism in *fcc* alloys.

Appendix A. Stress field of a dilatation line

Considering that hydrogen atoms are separated by a distance δ along the dilatation line shown on Fig. 9, in plane strain, the dilatation ΔV induced by the presence of $1/\delta$ hydrogen atoms per unit length is:

$$\Delta V = \frac{1}{\delta}\cdot\frac{\Omega}{2(1-\nu)} \tag{A1}$$

where $\Omega = V^*/N_{\mathrm{av}}$ is the unconstrained volume dilatation due to one atom. This volume change around the line turns into a radial displacement field **u**. The volume contained in the wall of a cylinder of radius r and wall thickness u_r is ΔV (Fig. 9):

$$\Delta V = 2\pi r\cdot u_r \tag{A2}$$

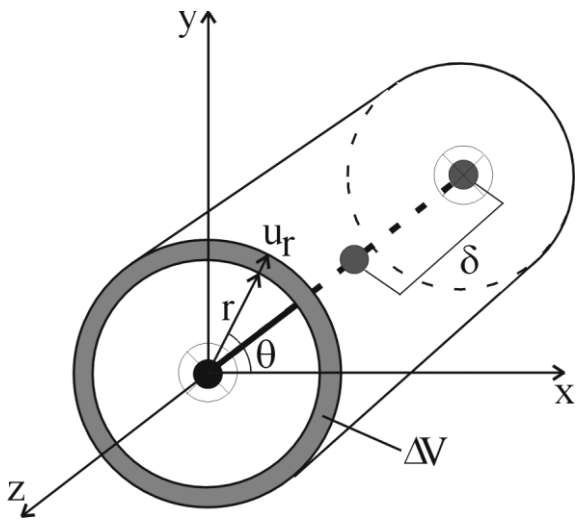

Fig. 9. Volume dilatation and displacement field of a dilatation line.

The displacement field and strain tensor are:

$$\begin{cases} u_r = \dfrac{V^*}{4\pi(1-\nu)\delta N_{av}} \dfrac{1}{r} \\ u_\theta = 0 \end{cases} \quad \text{(A3)}$$

$$\begin{cases} \varepsilon_{rr} = -\dfrac{V^*}{4\pi(1-\nu)\delta N_{av}} \dfrac{1}{r^2} \\ \varepsilon_{\theta\theta} = \dfrac{V^*}{4\pi(1-\nu)\delta N_{av}} \dfrac{1}{r^2} \\ \varepsilon_{r\theta} = 0 \end{cases} \quad \text{(A4)}$$

Hooke's laws gives:

$$\begin{cases} \sigma_{rr} = -\dfrac{\mu V^*}{2\pi(1-\nu)\delta N_{av}} \dfrac{1}{r^2} \\ \sigma_{\theta\theta} = \dfrac{\mu V^*}{2\pi(1-\nu)\delta N_{av}} \dfrac{1}{r^2} \\ \sigma_{r\theta} = 0 \end{cases} \quad \text{(A5)}$$

Expressing Eq. (A5) in the (x_1,x_2) plane and changing the co-ordinates into the independent system $z = x_1 + i.x_2$, $\bar{z} = x_1 - i.x_2$ (where $i = \sqrt{-1}$) gives:

$$\begin{cases} \sigma_{11} = -\dfrac{\mu V^*}{4\pi(1-\nu)\delta N_{av}} \left(\dfrac{1}{z^2} + \dfrac{1}{\bar{z}^2} \right) \\ \sigma_{22} = \dfrac{\mu V^*}{4\pi(1-\nu)\delta N_{av}} \left(\dfrac{1}{z^2} + \dfrac{1}{\bar{z}^2} \right) \\ \sigma_{12} = -\dfrac{\mu V^*}{4\pi(1-\nu)i\delta N_{av}} \left(\dfrac{1}{z^2} - \dfrac{1}{\bar{z}^2} \right) \end{cases} \quad \text{(A6)}$$

The equilibrium equations expressed in the complex plane reads:

$$\frac{\partial}{\partial z}(\sigma_{22} - \sigma_{11} + 2i\sigma_{12}) + \frac{\partial}{\partial \bar{z}}(\sigma_{11} + \sigma_{22}) = 0 \quad \text{(A7)}$$

The terms in brackets derive from a complex potential $\Phi(z,\bar{z})$. Two complex functions $\varphi(z)$ and $\psi(z)$ exist, such that:

$$2\mu u = (3-4\nu)\varphi - z\bar{\varphi} - \bar{\psi}$$

$$\begin{cases} \sigma_{11} + \sigma_{22} = 2(\varphi' + \bar{\varphi}) \\ \sigma_{22} - \sigma_{11} + 2i\sigma_{12} = 2(\bar{z}\varphi'' + \psi') \end{cases} \quad \text{(A8)}$$

The complex potential $\omega(z) = z\varphi'(z) + \psi(z)$ is introduced to take the presence of a crack into account in a further development. Eq. (A8) becomes:

$$2\mu u = (3-4\nu)\varphi - (z-\bar{z})\bar{\varphi} - \bar{\omega}$$

$$\begin{cases} \sigma_{11} + \sigma_{22} = 2(\varphi' + \bar{\varphi}) \\ \sigma_{22} - i\sigma_{12} = \varphi' + \bar{\omega}' + (z-\bar{z})\bar{\varphi}' \end{cases} \quad \text{(A9)}$$

Calculated in an infinite homogeneous matrix, the complex potentials of a dilatation line are:

$$\begin{cases} \varphi'_H(z) = 0 \\ \omega'_H(z) = \dfrac{B}{(z-\xi)^2} \text{ with } B = \dfrac{\mu V^*}{2\pi(1-\nu)\delta N_{av}} \end{cases} \quad \text{(A10)}$$

The associated displacement and stress fields are derivated:

$$u = \frac{B}{4\mu(\bar{z}-\bar{\xi})}$$

$$\begin{cases} \sigma_{11} + \sigma_{22} = 0 \\ \sigma_{22} + i\sigma_{12} = \dfrac{B}{(z-\xi)^2} \end{cases} \quad \text{(A11)}$$

where ξ is the complex coordinate of the line.

For box '*j*', the distance δ_j between hydrogen atoms along its equivalent dilatation line depends on C_j and the box size h. The number of hydrogen atoms along the line defect per unit length is equal to the number of hydrogen atoms in the box:

$$\frac{1}{\delta_j} = (1 \cdot h^2)(C_j N_{\text{av}}) \quad \text{(A12)}$$

And the stress induced by hydrogen in box j is given by Eq. (A11), with:

$$B_j = \frac{\mu V^* C_j h^2}{2\pi(1-\nu)} \quad \text{(A13)}$$

Appendix B. Force exerted by a dilatation line on an edge dislocation

Consider a dislocation at a position ζ and a dilatation line at a position ξ_i. To calculate the force exerted by the dilatation line on the dislocation, we use Eshelby's expression. In two dimensions, the force per dislocation unit length is:

$$f_m = \oint_{(S)} \left(\frac{\sigma_{k1}u_{k,1}}{2}\delta_{im} - \sigma_{ij}u_{j,m}\right) \mathrm{d}S_i \quad m,i,j = 1,\ldots,2 \quad \text{(B1)}$$

where (S) is any cylindrical surface enclosing ζ but not ξ_i (Fig. 10) and σ and $\vec{u}$ are the total stress and displacement fields (i.e. the sum of the fields of the dilatation and the dislocation line). The surface (S) simplifies to a closed contour (C) centred at ζ., If t is the current complex point along the contour (C), $\mathrm{d}t = \mathrm{d}S_1 - i.\mathrm{d}S_2$. Inserting expressions (A9) of the stress and displacement fields in equation Eq. (B1), one may obtain $\bar{f} = f_1 - i.f_2$ defined by:

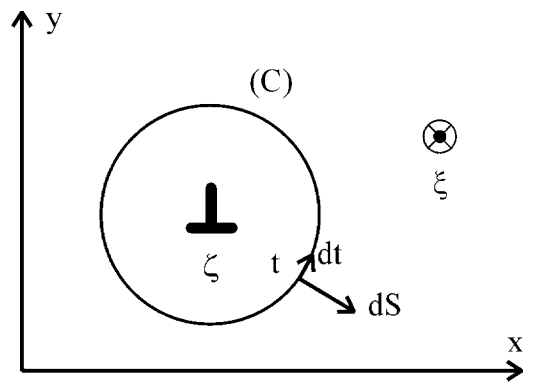

Fig. 10. Dislocation, dilatation line and integration path for the calculation of their interaction force.

$$\bar{f} = \frac{2\pi(1-\nu)}{\mu}[2\,\mathrm{Res}_\zeta\{\varphi'_{\text{tot}}\omega'_{\text{tot}} - \varphi'^2_{\text{tot}} - z\varphi'_{\text{tot}}\varphi''_{\text{tot}}\} + \mathrm{Res}_\zeta\{\varphi'^2_{\text{tot}}\}] \quad \text{(B2)}$$

where $(\varphi,\omega)_{\text{tot}} = (\varphi,\omega)_{\text{dislo}} + (\varphi,\omega)_{\text{Hline}}$

$Res_\zeta\{g\}$ is the enclosed residue of the complex function g in $t = \zeta$. It is defined by:

$$\oint_{(C)} g(t)\mathrm{d}t = 2\pi i \mathrm{Res}_\zeta\{g\} \quad \text{(B3)}$$

It is independent of the closed contour (C) and is non-zero only if ζ is a singularity for g. The position of the dilatation line is a singularity for the stress and displacement fields. Thus, ζ is a pole for g and the residues are calculated with the expression:

$$\mathrm{Res}_\zeta\{g\} = \lim_{t\to\zeta}\left\{\frac{1}{(m-1)!}\frac{\mathrm{d}^{m-1}}{\mathrm{d}t^{m-1}}[(t-\zeta)^m g(t)]\right\} \quad \text{(B4)}$$

where m is the order of the pole ζ. The complex potentials of the dilatation line are given by Eq. (A10), and the complex potentials of a dislocation are:

$$\begin{cases} \varphi'_D(z) = \dfrac{2A}{z-\zeta} \\ \omega'_D(z) = \dfrac{2\bar{A}}{z-\zeta} - \dfrac{2(\zeta-\bar{\zeta})A}{(z-\zeta)^2} \end{cases} \quad \text{(B5)}$$

with $b_e = b_1 + ib_2$; $A = \dfrac{\mu b_e}{8\pi i(1-\nu)}$

Eq. (B2), simplifies to:

$$\bar{f} = \frac{4\pi(1-\nu)}{\mu}\,\mathrm{Res}_{\zeta}\left\{\frac{2A \quad B_j}{(z-\zeta)(z-\xi_i)^2}\right\} \tag{B6}$$

where ζ is a first order pole. Finally, the force exerted by the dilatation line j on the dislocation is given by:

$$\bar{f} = \frac{\mu V^* C_j h^2 b_e}{2\pi i(1-\nu)(\zeta-\xi_j)^2} \tag{B7}$$

References

[1] Magnin T. Advances in corrosion–deformation interactions. Zurich: TransTech Publications, 1996.
[2] Magnin T, editor. Corrosion–deformation interactions. Proceedings CDI'96, Nice, France, 21. London: The Institute of Materials; 1996.
[3] Ulmer DG, Altstetter CJ. In: Moody NR, Thompson AW, editors. Hydrogen effects on material behaviour. Jackson Lake Lodge, WY: TMS; 1989. p. 421–30.
[4] Quiao L, Chu M, Mao X. Corr. Sci. 1996;52(4):275–9.
[5] Englemann HJ, Mummert K, Schwartz S, Uhlemann M. In: Turnbull A, editor. Hydrogen transport and cracking inp metals. London, UK: The Institute of Materials, 1994, p. 27–37.
[6] Delafosse D, Magnin T. Eng Frac Mech 2001;68(6):693–729.
[7] Birnbaum HK, Sofronis P. Mater Sci Engng A 1994;176:191–202.
[8] Birnbaum HK, Robertson IM, Sofronis P, Teter D. In: Magnin T, editor. 2nd International Conference on Corrosion–Deformation Interactions CDI'96, Nice, France. London: The Institute of Materials; 1996. p. 172–95.
[9] Brass AM, Chene J. Mater Sci Engng A 1998;242:210–21.
[10] Magnin T, Chambreuil A, Bayle B. Acta Mater 1996;44(4):1457–70.
[11] Sofronis P. J. Mech. Phys. Solids 1995;43(9):1385–407.
[12] Sofronis P, Birnbaum HK. J. Mech. Phys. Solids 1995;43(1):49–90.
[13] Chene J, Brass AM. In: Desjardins D, Oltra R, editors. Corrosion sous contrainte. Phénoménologie et mécanismes. Les Ulis (France): Les Editions de Physique; 1990. p. 159–210.
[14] Van Leeuwen HP. Eng. Frac. Mech. 1974;6:141–61.
[15] Eshelby JD. Proc. Roy. Soc. A 1957;241:376–96.
[16] Hirth JP, Lothe J. Theory of dislocations. Malabar, FL: Krieger Publishing Co, 1992.
[17] Cottrell AH, Jawson MA. Proc. Roy. Soc. A 1949;199:104.
[18] Lin HI, Thomson R. Acta Metall. Mater. 1986;34(2):187–206.
[19] Donovan JA. Metal. Mater. Trans. A 1976;7:1677.
[20] Englemann HJ, Schwartz S, Uhlemann M, Mummert K. In: Magnin T, editor. 2nd International Conference on Corrosion–Deformation Interactions CDI'96, Nice, France. London: The Institute of Materials; 1996. p. 238–47.
[21] Bonneville J, Escaig B. Acta Metall. 1979;27:1477–86.
[22] Combette P, Grilhé J. Mém. Sci. Rev. Métall. 1970;LXVII(7–8):491–505.
[23] Windle AH, Smith GC. Met. Sci. J. 1968;2:187–91.
[24] Boniszewski T, Smith GC. Acta Metall. 1963;11:165–78.
[25] Wilcox BA, Smith GC. Acta Metall. 1965;13:331–43.
[26] Robertson IM. Eng. Frac. Mech. 1999;64:649–73.
[27] Eastman J, Heubaum F, Matsumoto T, Birnbaum HK. Acta Metall. 1982;30:1579–86.
[28] Sirois E, Birnbaum HK. Acta Metall. Mater. 1992;40(6):1377–85.
[29] Magnin T, Bosch C, Wolski K, Delafosse D. Mat. Sci. Eng. A 2001;314(1–2):7–11.
[30] Abraham DP, Altstetter CJ. Metal. Mater. Trans. A 1995;26:2849–58.
[31] Ferreira PJ, Robertson IM, Birnbaum HK. In: Intergranular and interphase boundaries in materials. Switzerland: TransTech Publications; 1996. p. 93–6.
[32] Ferreira PJ, Robertson IM, Birnbaum HK. Acta Mater 1999;47(10):2991–8.